

Nanobubbles from Gas-Generating Polymeric Nanoparticles: Ultrasound Imaging of Living Subjects**

Eunah Kang, Hyun Su Min, Jaeyoung Lee, Moon Hee Han, Hyung Jun Ahn, In-Chan Yoon, Kuiwon Choi, Kwangmeyoung Kim, Kinam Park, and Ick Chan Kwon*

Ultrasound (US) is a noninvasive biomedical imaging modality that is widely available, inexpensive, safe, and provides real-time imaging and diagnosis. US contrast enhancement improves the image quality because of acoustic impedance mismatch, which can occur when a liquid or gas is encapsulated within shell materials or when liquid or solid particles with a high density difference are brought together.^[1–3] Microbubbles were primarily used as US contrast agents for blood flow imaging, however, development of metabolic or molecular US imaging that employs microbubbles has been limited because sub-microbubbles or nanoparticles that are appropriate for tissue penetration have poor echogenic sensitivity, while nanoparticles can not be visualized at the resolution of US imaging instruments (typically 50 to 100 μm).^[4]

Recently, nanoparticles have been employed in numerous biomedical applications.^[5] Nanoparticles bypass the reticuloendothelial system, and allow prolonged circulation and passive localization within tumor vasculature by tissue extravasation and enhanced permeation and retention (EPR).^[6] Moreover, nanoparticles can be modified by addition of ligands that increase nanoparticle affinity toward specific target sites, such as tumors.^[7,8] In addition, the insertion of protease cleavage sites can provide activatable imaging probes,^[9] thus allowing simultaneous molecular imaging and therapeutics. The need to use nanosized carriers for in vivo imaging and therapy has led to the development of laser-induced photoacoustic US^[10,11] and to the exploration of materials-based approaches that employ perfluorocarbon-

encapsulated lipid-based nanoparticles^[12] and polymeric micelles.^[13]

Herein, we describe the generation of nanobubbles, which can be imaged by US and are derived from gas-generating polymeric nanoparticles (GGPNPs). The proposed mechanism involves localization of echogenic GGPNPs in a tumor and coalescence of generated nanobubbles, followed by fusion of nanobubbles into microbubbles. Significantly, we produced GGPNP nanobubbles without encapsulation of a gas precursor (perfluorocarbon). Instead, in our system, the GGPNP carbonate side chain is degraded to form carbon dioxide. The mechanism appears to involve diffusion of water into the GGPNPs, cleavage of the carbonate side chains by hydrolysis, and formation of carbon dioxide nanobubbles on the GGPNP surface, followed by expansion or coalescence of nanobubbles into microbubbles. The resulting microbubbles exhibit resonance under a US field (Figure 1 a).

Polyesters with carbonate side chains (poly(BL-PO)) were synthesized by ring-opening copolymerization of γ -butyrolactone and propylene oxide using samarium diiodide as initiator (Figure S1b in the Supporting Information).^[14,15] The carbonate side chains were created by conjugation with hydroxy groups of hydroxy γ -butyrolactone and cholesteryl chloroformate or ethyl chloroformate (Figure S1–S3 in the Supporting Information). The copolymerization ratios of cholesteryl carbonate γ -butyrolactone and ethyl carbonate γ -butyrolactone were varied with respect to that of propylene oxide. The resulting chemical structures are shown in Figure 1 b. The initial feed ratios of three monomers were 1:2:1 for poly(BL-PO). The actual ratio of three monomer units in the poly(BL-PO) was confirmed as 1:1.74:0.81 by ¹H NMR spectroscopy (see Figure S4 in the Supporting Information). This result shows that the compositions of the copolymers were well-matched to the initial feed ratio. The presence of the cholesteryl group means that the relative proportions of cholesteryl carbonate and ethyl carbonate determine the physical stability of the polymer. The hydrolyzed particles produce biocompatible water, carbon dioxide, cholesterol, and ethanol. To prove the biocompatibility of our particles, we examined their effect on cell viability. At a concentration of up to 1 mg mL^{-1} , our particles were not cytotoxic (see Figure S8 in the Supporting Information).

Nanoparticles generated from poly(BL-PO) (1:2:1) were termed GGPNPs. Dynamic light scattering (DLS) indicated that the average GGPNP diameter was 581 nm (Figure S6 in the Supporting Information), and transmission electron microscopy (TEM) indicated that the GGPNP morphology was spherical and the diameter was less than 500 nm (Figure 1 c). The size appeared larger by DLS probably

[*] Dr. E. Kang,^[†] H. S. Min,^[†] Dr. H. J. Ahn, Dr. I. C. Yoon, Dr. K. Choi, Dr. K. Kim, Dr. I. C. Kwon
Biomedical Research Center

Korea Institute of Science and Technology
39-1 Hawolgok-dong, Seongbuk-gu, Seoul 136 791 (Korea)
Fax: (+82) 2-958-5909
E-mail: ikwon@kist.re.kr

Dr. J. Lee, Dr. M. H. Han
Department of Radiology, Seoul National University Hospital
101 Daehangno, Jongno-gu, Seoul 110-744 (Korea)

Dr. K. Park
Department of Biomedical Engineering and Pharmaceutics
Purdue University, West Lafayette, IN 47906 (USA)

[†] These authors contributed equally to this work.

[**] This work was financially supported by the Real-Time Molecular Imaging Project, 2009K001594, the GRL Program of MEST, and by grants from the Intramural Research Program of KIST (Theragnosis) and the Ministry of Health Welfare and Family Affairs (A062254).

Supporting information for this article is available on the WWW under <http://dx.doi.org/10.1002/anie.200903841>.

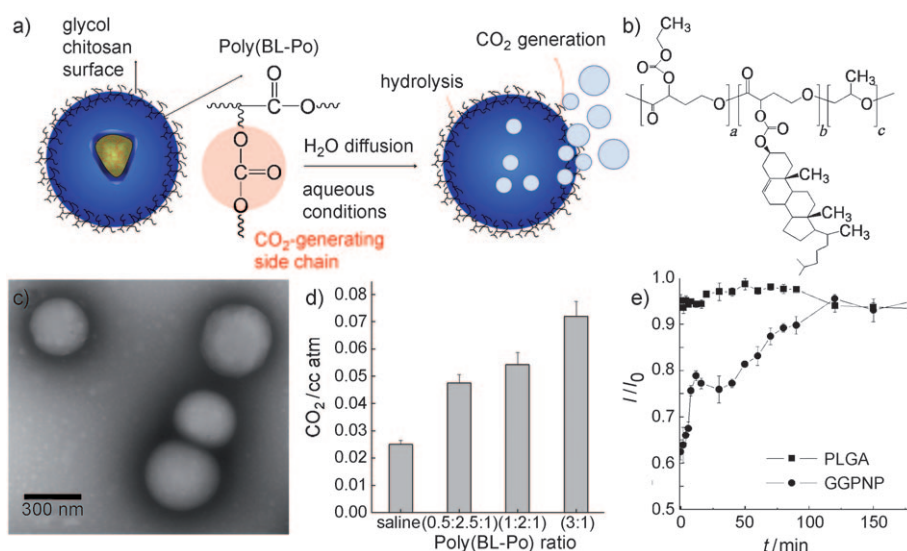


Figure 1. a) Illustration of gas-generating polymeric nanoparticles. b) Chemical structure of poly(BL-PO). c) Spherical HGC-coated gas-generating polymeric nanoparticles of poly(BL-PO) (1:2:1). d) The amount of carbon dioxide from poly(BL-PO) nanoparticles generated after 5 min exposure. e) The transmitted ultrasound intensity of PLGA NP and GGPNP (I_0 is the ultrasound intensity of PBS) as a function of time at 37°C.

because bubbles were produced on the GGPNP surfaces. GGPNPs of the appropriate diameter were prepared so that they might accumulate in tumors by EPR. The hydrophobic surface was rendered passive using hydrophobically modified glycol chitosan (HGC) with a 17% substitution ratio of cholanic acid as a surfactant. It is presumed that the positive charges on the HGC units provided a tumor affinity, so that the nanoparticles could accumulate therein.^[15] We used mass spectrometry to measure the generation of carbon dioxide from GGPNPs following their dispersal in saline for 5 min (to allow hydrolysis). Carbon dioxide release was then measured by monitoring the peak at 44 Da (Figure S7 in the Supporting Information). Based on calibrations of volume and pressure, the amount of residual carbon dioxide present in saline (0.025 cc atm) and the amount of GGPNP-generated carbon dioxide in saline were quantified by using mass spectrometry (Figure 1d). The latter levels were 0.048, 0.052, and 0.074 cc atm for copolymerization ratios of cholesteryl:ethyl carbonate of 0.5:2.5, 1:2, and 3:1, respectively. Thus, the amount of GGPNP-generated carbon dioxide was 1.92, 2.08, and 2.96 times greater than that of intrinsic carbon dioxide. In vitro and in vivo characterization of GGPNPs as a US contrast agent employed poly(BL-PO) (1:2:1). The acoustic characteristic and bubble

stability of GGPNP at 37°C were observed using the transmitted ultrasound intensity (Figure 1e), which reflects the lifetime of the microbubbles under US irradiation.^[17,18] The curve for GGPNPs presented an initially rapid intensity increase up to 12.5 min, which indicated that initially generated gas bubbles from GGPNPs rapidly burst under US irradiation. However, the intensity then decreased slightly until 41 min, thus implying that GGPNPs may continuously and rapidly generate a large amount of bubbles over this time period. Interestingly, GGPNPs showed a prolonged lifetime of the gas bubbles (>1 h) compared to microbubbles with a phospholipid shell (ca. 5 min).^[17] As expected, the control poly(lactide-co-glycolic acid) (PLGA) NPs do not present any change of the transmitted ultrasound intensity under US irradiation.

To investigate the hydrolysis mechanism of GGPNPs in PBS at 37°C, we measured the changes of particle size and morphology by using DLS and TEM. From the DLS measurements, GGPNPs showed an increased particle size of about 640 nm at 1 min post-incubation (Figure 2a) compared to the size of 200–500 nm for freshly prepared GGPNPs (Figure 1c), thus indicating that bubbles were rapidly produced on the GGPNP surfaces (Figure 2c). At 30 min post-incubation, a large number of microbubbles (>1 μm) were observed, thus indicating that the hydrolyzed GGPNPs produced microsized bubbles. As expected, the TEM micrographs showed some surface erosion at 1 min post-incubation of GGPNPs in PBS at 37°C, and this surface erosion increased with incubation times up to 30 min. Importantly, after 2 h post-incubation, most of the polymers in the core

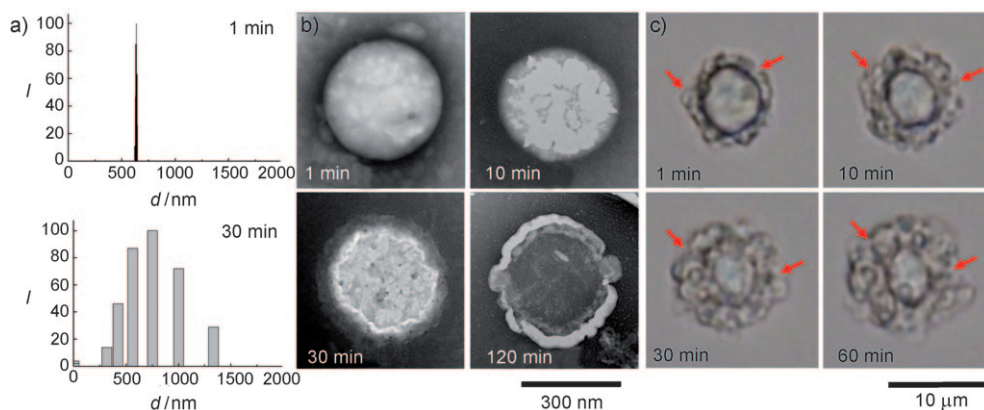


Figure 2. a) Size distribution of GGPNPs incubated in PBS at 37°C for 30 min measured using DLS. b) TEM micrographs of GGPNPs hydrolyzed in PBS for 2 h at 37°C. c) Optical micrograms of gas-generating profiles of microsized GGPNPs (6–8 μm) incubated in PBS at 37°C for 1 h (arrows indicate gas-generating bubbles). Original magnification is ×400.

were degraded: the hydrolysis reaction might be auto-accelerated because of the higher concentration of CO₂ (Figure 2b). Finally, we directly visualized the gas generation profile of hydrolyzed GGNPs by using optical microscopy. To visualize the direct gas formation, we used gas-generating microparticles with an average size of about 6–8 μm, as the nanosized GGNPs were not observed using optical microscopy, but the microparticles had the same chemical composition and molecular weight of the GGNPs. Interestingly, within 1 min post-incubation in PBS, many small bubbles (< micrometer) were observed on the particle surface. As the incubation time increased up to 1 h, the small bubbles formed larger bubbles (> micrometer), because of the expansion or coalescence of nanobubbles into microbubbles. These gas-generation profile data were closely related to the hydrolysis pattern of gas-generating polymeric particles.

We performed in vitro comparisons of US contrast agents consisting of GGNPs and (control) PLGA nanoparticles employing US imaging equipment with 2D and cadence pulse sequence imaging modes, and a 15 MHz linear transducer (Figure 3a). The PLGA nanoparticles (negative control)

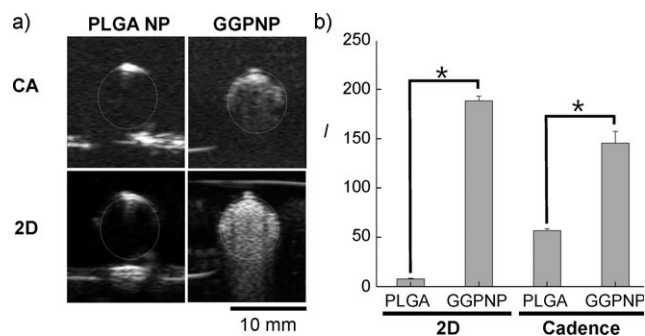


Figure 3. In vitro characterization of GGNP in aqueous conditions. a) US images of GGNP dispersion at 2D and cadence (CA) mode. b) Histogram of US intensity from PLGA and GGNP dispersions. The image was taken at under the same condition of gain = 10/MI = 0.5. * indicates significance level of $p < 0.05$. MI = mechanical index.

showed no acoustic reflectivity contrast under either mode because the resolution of US imaging is approximately 50–100 μm and the PLGA nanoparticles, which do not form bubbles, were not echogenic. In contrast, US contrast images of GGNP dispersions were significantly enhanced in both modes ($p < 0.05$; Figure 3b). The contrast enhancement that arises from GGNP dispersion in the cadence mode indicated that the presence of microbubbles or the coalescence of carbon dioxide nanobubbles was responsible for US resonance.

We subsequently investigated the feasibility of using GGNPs as an in vivo US contrast agent. We first administered GGNP dispersions (0.5–5.0% w/v) subcutaneously into the lower backs of BALB/c mice. US images were taken immediately after injection and the change in US contrast was observed over time by cadence pulse sequencing and 2D modes (Figure 4a). The results clearly showed that the intensity increased as a function of GGNP concentration (Figure 4c). Under the same conditions of gain, mechanical

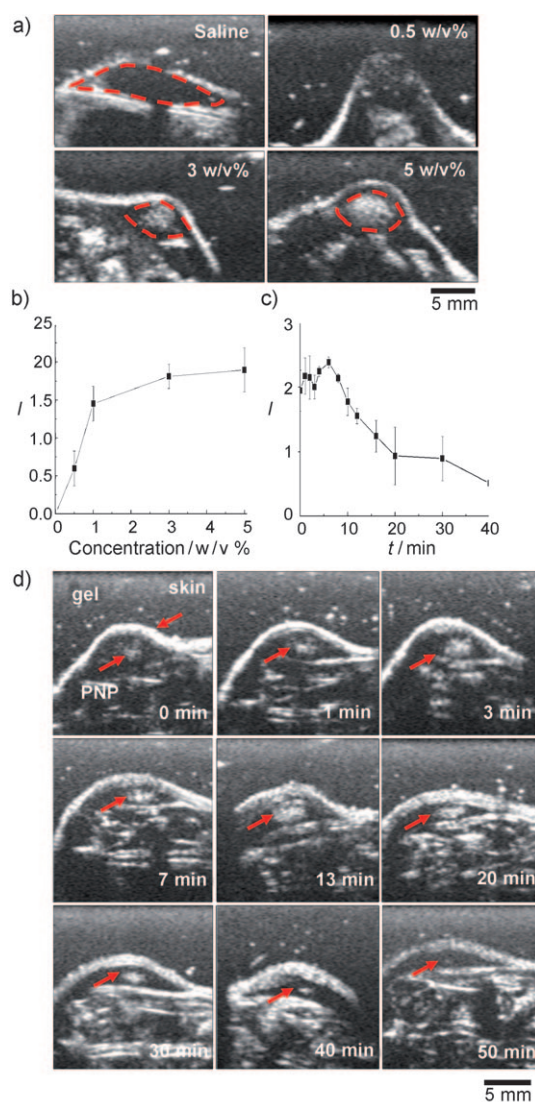


Figure 4. Ultrasound images aided by contrast agent administered by subcutaneous injection. All images were taken at cadence mode under the same condition of MI = 0.5/gain = 10. After subcutaneous injection, US images taken as a function of a) concentration and b) time at a concentration of 3 w/v%. Intensity profiles were presented as a function of c) concentration and d) time.

index, and power, the US intensity of the region of interest was normalized to the background intensity of ultrasound gel on the skin. The local area where the saline control was injected showed a clear margin with no contrast signal in the cadence mode, thus indicating the absence of acoustically reflective bubbles. However, a very small US contrast enhancement by GGNPs could be seen at a GGNP concentration of 0.5% w/v, which is presumably near the threshold of signal detection. As the GGNP concentration increased, the nanobubbles coalesced or merged into microbubbles and the signal became stronger. We also monitored the change in the US signal over time (Figure 4b). The US signal initially increased, maintained a plateau for approximately 10 min, and then gradually decreased (Figure 4d). The contrast enhancement of the cadence and 2D modes was

visible for 30 min, which should be sufficient to allow for in vivo real-time imaging. Notably, our results show that the cadence-mode US signal was caused by bubble resonance, and not by enhancement of 2D back-scattering. The presence of a signal in the cadence mode clearly indicates that the dispersion of polymeric nanoparticles generated coalesced nanobubbles of carbon dioxide and that the resulting microbubbles vibrated under the applied US field.

To demonstrate US imaging of a tumor, we administered an intratumoral injection of 3% w/v GGNP dispersion to tumor-xenograft-bearing BALB/c mice and compared US images pre- and post-injection (Figure 5). The US intensity at

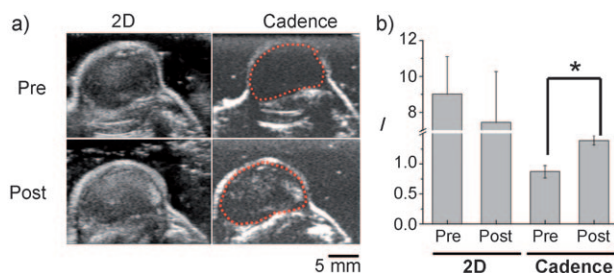


Figure 5. Contrast enhancement of a tumor before (pre) and after (post) intratumoral injection. a) US images taken at both 2D and cadence mode. b) Histogram of normalized intensities derived from the images. * indicate a significance level of $p < 0.05$.

the tumor site was weak compared with that seen after subcutaneous injection because of the rapid leakage of GGNPs into blood vessels after injection. However, immediately after injection and for the following 1 min, we observed localized spots of enhanced contrast in the tumor by the cadence mode. A comparison of contrast enhancement in the 2D and cadence modes indicated a significant intensity difference of in the cadence mode pre- and post-injection ($p < 0.05$). The US intensity in the cadence mode increased by 58% after intratumoral administration, whereas the intensity in the 2D mode was not significantly enhanced. The appearance of local spots of enhanced contrast suggests that adequate accumulation of GGNPs occurred at the tumor site, thus allowing US imaging. Therefore, the GGNPs penetrated the tumor interstitium, coalesced to form nanobubbles, and provided a vibrating reactivity visible under the cadence mode of US. As the resolution of our US instrument is approximately 100 μm , we could not resolve nanobubbles. The localized spots clearly visible in the tumor indicated that nanobubbles generated from gas-generating nanoparticles had coalesced into microbubbles. Our results indicate that GGNPs can generate nanobubbles that coalesce into microbubbles, which resonate under a US field. GGNPs have great potential as contrast agents that can facilitate in vivo US imaging.

Experimental Section

Materials: Samarium, 1, 2-diiodoethane, sodium thiosulfate solution, pyridine, α -hydroxy- γ -butyrolactone, cholesteryl chloroformate, and

propylene oxide were purchased from Sigma Chemical Co. (St. Louis, MO).

Polymerization of poly(butyrolactone-co-propylene oxide) with a pendant cholesteryl/ethyl carbonate group: Detailed procedures are described in the Supporting Information. Briefly, α -hydroxy- γ -butyrolactone and either cholesteryl chloroformate or ethyl chloroformate were dissolved in dichloromethane. The mixture was placed in an ice bath and pyridine was added dropwise under stirring. After 20 h at room temperature, the solution was washed with 1M HCl, saturated NaHCO_3 , and distilled water, and precipitated by addition of cold ethyl ether. The resulting white crude powder was isolated and dried under vacuum. The yield was 85.4%.

Polymerization of poly(butyrolactone-co-propylene oxide) with a pendant cholesteryl/ethyl carbonate group was performed by initiation with samarium diiodide/samarium (SmI_2/Sm). Different monomer ratios of γ -butyrolactone with a cholesteryl carbonate or ethyl carbonate pendant group and propylene oxide (PO) were dissolved in toluene. Following addition of SmI_2/Sm , the mixture was stirred at 100°C under reduced pressure (0.1 Torr). After 48 h, the product was precipitated by addition of cold ethyl ether and filtered. The resulting crude powder was dried under vacuum. The yield of poly(BL-PO) was 68.23%.

Particle preparation and morphology: Nanoparticles were synthesized by emulsification of the oil-in-water phase using a probe sonicator. An HGC solution (0.2% w/v) was used as the water phase (10 mL of fluid). A polymer solution (6% w/v) in dichloromethane (1 mL) was added dropwise into the water phase. After sonication, the particle dispersion was stirred for 2 h to remove residual solvent. After centrifugation, particles were redispersed in Tween 20 (0.5% w/v) and maltose (5% w/v; disintegration agent in reconstitution) and freeze-dried. The dried powder was resuspended at the desired concentration prior to use. The particle morphology and diameter were determined using DLS (Spectra Physics, Mountain View, CA) and TEM (CM-200, Philips, CA).

The carbon dioxide content of GGNPs were measured using a quadrupole mass spectrometer (Prisma QME 200, Germany) equipped with a Faraday cup detector. The vapor was analyzed with an emission current of 1.5 mA, an electron energy of 10 eV, and a resolution of 50. Saline (3 mL) and GGNPs (20 mg) were placed in a gas-tight syringe. As a control, dissolved gas species in saline alone were measured. The gas generated from GGNPs after hydrolysis was quantified after 5 min exposure to saline.

In vitro acoustic measurements were performed by detecting attenuation signals of GGNPs exposed to a focused ultrasound pulse (10 MHz), as described previously.^[18] Briefly, the dispersed GGNPs in phosphate-buffered saline (PBS; 3%, w/v) were placed in a 50 mL acrylic chamber located between an immersing type 10 MHz transducer (12.7 mm diameter, V311, Panametrics Inc., Waltham, MA) and a home-made metallic reflector in a 37°C water bath with gentle stirring. This experiment was repeated 5 times. A pulse of ultrasound was sent to the sample chamber and then the reflected pulse was observed using a pulser/receiver. The reflected pulse was converted to radiofrequency (RF) signals using a digital oscilloscope (Ultrawave-2020, MKC Korea Inc., Korea). The RF signals of GGNPs were processed by fast Fourier transform (FFT) and filtered using the LabView program (National Instruments Corp., TX). Attenuation spectra were obtained by dividing the GGNPs values in the vicinity of the FFT maxima by the values of pure PBS under the same conditions.

Hydrolysis test: GGNPs (1 mg mL⁻¹) were dissolved in PBS and incubated 2 h at 37°C. Under these hydrolysis conditions, the changes in particle size and morphology were characterized using DLS and TEM according to the incubation time. To directly visualize the gas-bubbling profile of GGNPs, we made gas-generating microparticles with an average size of about 6–8 μm using a homogenizer with 15000 rpm. The microparticles have the same chemical composition and molecular weight of GGNPs. After incubating microparticles in

PBS, the time-dependent gas-generating profile was monitored in situ using optical microscope equipped with 40× focal lens (BX51; Olympus Co. Ltd., Japan).

In vitro US imaging was performed in the static state. Eppendorf tubes were embedded in agarose gel (3%, w/v) and GGNP dispersions (0–5%, w/v) were placed into the tubes. As negative controls, US contrast agents consisting of PLGA nanoparticle dispersions at the same concentrations were employed. US was performed in the 2D and cadence pulse sequencing (CPS) modes. US imaging (Acuson Sequoia 512 system; Siemens Medical Solutions, Malvern, PA) was achieved using a 15 MHz probe (Acuson model 15 L8). Statistical analysis employed the Tukey method of one-way analysis of variance (ANOVA). A *p* value less than 0.05 was considered significant.

In vivo ultrasound imaging: All animal experiments were performed according to the Guidelines for Care and Use of Research Animals developed by the Seoul National University Animal Study Committee. Male BALB/c mice (*n* = 3, 25–30 g body weight) less than 6 weeks old were anesthetized using isoflurane gas (2–3%, v/v). Lower back hair was removed with depilatory cream and each animal received a subcutaneous inoculation of 1×10^6 squamous cell carcinoma (SCC7) cells in the lower back. Cells were obtained from the American Type Culture Collection (ATCC) and suspended in 50 μL of medium. Xenograft tumor-bearing mice with tumor volumes of approximately 1500 mm³ (calculated by $[ab^2]/2$) were given intratumoral injections of a GGNP dispersion (3%, w/v) at four sites around the tumor. The total received dose was 100 μL.

Received: July 14, 2009

Revised: November 3, 2009

Published online: December 9, 2009

Keywords: carbon dioxide · imaging agents · nanostructures · polymers · ultrasound

[1] S. P. Qin, C. F. Caskey, K. W. Ferrara, *Phys. Med. Biol.* **2009**, *54*, R27–R57.

- [2] K. Ferrara, R. Pollard, M. Borden, *Annu. Rev. Biomed. Eng.* **2007**, *9*, 415–447.
- [3] E. G. Schutt, D. H. Klein, R. M. Mattrey, J. G. Riess, *Angew. Chem.* **2003**, *115*, 3336–3355; *Angew. Chem. Int. Ed.* **2003**, *42*, 3218–3235.
- [4] J. R. Lindner, *Nat. Rev. Drug Discovery* **2004**, *3*, 527–532.
- [5] G. S. Kwon, M. Naito, M. Yokoyama, T. Okano, Y. Sakurai, K. Kataoka, *Pharm. Res.* **1995**, *12*, 192–195.
- [6] Y. Takakura, R. I. Mahato, M. Hashida, *Adv. Drug Delivery Rev.* **1998**, *34*, 93–108.
- [7] S. Keren, C. Zavaleta, Z. Cheng, A. de La Gheysens, S. S. Gambhir, *Proc. Natl. Acad. Sci. USA* **2008**, *105*, 5844–5849.
- [8] G. E. Weller, M. K. Wong, R. A. Modzelewski, E. Lu, A. L. Klibanov, W. R. Wagner, F. S. Villanueva, *Cancer Res.* **2005**, *65*, 533–539.
- [9] R. Weissleder, C. H. Tung, U. Mahmood, A. Jr Bogdanov, *Nat. Biotechnol.* **1999**, *17*, 375–378.
- [10] K. H. Song, C. Kim, C. M. Cobley, Y. Xia, L. V. Wang, *Nano Lett.* **2009**, *9*, 183–188.
- [11] X. Wang, Y. Pang, G. Ku, X. Xie, G. Stoica, L. V. Wang, *Nat. Biotechnol.* **2003**, *21*, 803–806.
- [12] F. S. Villanueva, W. R. Wagner, *Nat. Clin. Pract. Cardiovasc. Med.* **2008**, *5* Suppl 2, S26–32.
- [13] N. Rapoport, Z. G. Gao, A. Kennedy, *J. Natl. Cancer Inst.* **2007**, *99*, 1095–1106.
- [14] S. Agarwal, X. Xie, *Macromolecules* **2003**, *36*, 3545–3549.
- [15] M. Nishiura, Z. Hou, T. A. Koizumi, T. Imamoto, Y. Wakatsuki, *Macromolecules* **1999**, *32*, 8245–8251.
- [16] K. Park, J. H. Kim, Y. S. Nam, S. Lee, H. Y. Nam, K. Kim, J. H. Park, I. S. Kim, K. Choi, S. Y. Kim, I. C. Kwon, *J. Controlled Release* **2007**, *122*, 305–314.
- [17] S. Rossi, G. Waton, M. P. Krafft, *ChemPhysChem* **2008**, *9*, 1982–1985.
- [18] F. Gerber, M. P. Krafft, G. Waton, T. F. Vandamme, *New J. Chem.* **2006**, *30*, 524–527.